



Fermi National Accelerator Laboratory

FERMILAB-Pub-92/155

## A Phototube RICH Detector

M. Pommot Maia

*Conselho Nacional de Pesquisas  
Brazil*

P.S. Cooper and L. Stutte

*Fermi National Accelerator Laboratory  
P.O. Box 500, Batavia, Illinois 60510*

V. Solyanik

*Institute of High Energy Physics  
Serpukhov, Russia*

I. Filimonov and A. Nemitkin

*Moscow State University  
Russia*

June 1992

Submitted to *Nuclear Instruments and Methods*

## **Disclaimer**

*This report was prepared as an account of work sponsored by an agency of the United States Government. Neither the United States Government nor any agency thereof, nor any of their employees, makes any warranty, express or implied, or assumes any legal liability or responsibility for the accuracy, completeness, or usefulness of any information, apparatus, product, or process disclosed, or represents that its use would not infringe privately owned rights. Reference herein to any specific commercial product, process, or service by trade name, trademark, manufacturer, or otherwise, does not necessarily constitute or imply its endorsement, recommendation, or favoring by the United States Government or any agency thereof. The views and opinions of authors expressed herein do not necessarily state or reflect those of the United States Government or any agency thereof.*

# A Phototube RICH Detector

M. Pommot Maia\*

Conselho Nacional de Pesquisas - Brazil

P. S. Cooper, L. Stutte

Fermi National Accelerator Laboratory<sup>†</sup>

V. Solyanik

Institute of High Energy Physics, Serpukhov - Russia

I. Filimonov, A. Nemitkin

Moscow State University - Russia

June 3, 1992

## Abstract

The results from a prototype for a fast RICH detector using phototubes are presented, testing three different types of tubes in the photocathode. In a 400 GeV/c  $\pi^-$  beam, the number of photons detected was 11.8 per ring and the ring radius resolution obtained was 1.13%. The Figure of Merit,  $N_0$ , for the entire photocathode was measured to be 93/cm. Particle identification as a function of beam momentum was studied, as well as multiparticle event recognition.

---

\*Present address: Stanford University, Stanford, CA - 94309.

<sup>†</sup>Work supported by the U.S. Department of Energy under contract NO. DE - AC02 - 76CHO3000

The experiment **E781- SELEX: A Segmented Large  $x_F$  Baryon Spectrometer**, scheduled to collect data in the next fixed target run at Fermilab, will be performing high statistics studies of production mechanisms and decay physics of the four known charmed baryons,  $\Sigma_c$ ,  $\Xi_c$ ,  $\Omega_c$ ,  $\Lambda_c$ .

The physics goals of the experiment require, among other things, good charged particle identification to look for the different baryon decay modes. One must be able to separate  $\pi$ , K and p over a wide momentum range when looking for charmed baryon decays like  $\Lambda_c^+ \rightarrow p K^- \pi^+$ . A RICH[1] detector with a phototube photocathode array is proposed to do this. The E781 RICH detector design goals include high efficiency for detection of the produced photons and good ring radius resolution, in order to be able to separate pions and kaons up to 250 GeV/c.

Because the readout is phototube-based, it is necessarily fast. In addition, the output signal from the phototubes can be easily digitized to give a pixel readout and be available at trigger decision time.

## 1 Detector

The particles traverse a 10 m long radiator vessel filled with neon (99.99% purity) at 1 atm. By using this noble gas one avoids worrying about dispersion[2] in the radiator medium so that the ring radius resolution is determined by

the detector resolution.

The angular coverage is limited by the transmission of the fast particles through a magnet to be within  $\pm 20$  mrad vertically and  $\pm 65$  mrad horizontally. The produced photons are reflected by a spherical mirror (focal length 10 m) into a photomultiplier tube matrix array. Phototubes have a well known, large quantum efficiency. The tubes are mounted in hexagonally packed light cones to improve the light collection by increasing the areal coverage. They need to be small enough to give good resolution in ring radius. In order to cover the stated angular acceptance with the required resolution the matrix should have about 3000 tubes.

## 1.1 Prototype

A prototype with 10% of the number of tubes was built to test these ideas. It is shown schematically in Figure 1-a. A 10 m long, 1 m diameter vessel[3] was filled with neon at 1 atm, used as the radiator medium. The beam window was circular (25.4 cm diameter). The produced photons were reflected by a spherical (40.6 cm diameter) optical quality mirror and traveled to the phototube array located at its focal plane (10 m). The tubes could not be housed in a neon environment since neon has been shown[4] to penetrate the tube vacuum. The small volume in which they were located, filled with

nitrogen at atmospheric pressure, was separated from the radiator by a 6 mm quartz window.

The tests were performed during the 1991 fixed target run at Fermilab, running parasitically in the P-Center beam line. The main experiment, E800, used a 400 GeV/c negative hyperon beam to look for  $\Omega^-$  decays. The experimental setup is shown in Figure 1-b. Particle trajectories were determined by three PWC stations (22 planes, 4 views). The magnet was used to measure the particles' momenta. In addition, other detector prototypes, also shown in the figure, were tested: 8 planes of Silicon Microstrip Detectors and a Drift Chamber.

### 1.1.1 Phototube matrix

The tube holders, shown in Figure 2, were drilled from aluminum hexagonal stock, with one side of the holder housing the phototube and the other side forming the light-gathering cone. The cones were covered with thin aluminized mylar to increase their efficiency. The aluminized mylar improved the light collection by about 48%, also observed in previous studies[5]. The holders were then mounted in an aluminum support structure.

Three different phototubes were used in the array. The first were Hamamatsu model **R760**. The other two were manufactured in Russia: **FEU-60**

and FEU-68. The FEU-60 are a new generation of the ones used in the SPHINX[5] RICH detector. Listed in Table I are the characteristics for each tube type. A set of 122 R760, 64 FEU-60 and 101 FEU-68 was arranged in the matrix prototype, as in Figure 3-a.

## 1.2 Electronics

Both the R760 and FEU-60 bases have only a high voltage divider. However, the FEU-68 assemblies have a preamplifier, with a  $1 \mu\text{A}$  threshold, as well as a pulse former in a chip. The phototube signal is processed through a hybrid circuit which is a preamplifier, discriminator and line driver. The output is a differential ECL signal which can be fed directly into a latch readout. Similar hybrid circuit chips were provided for the R760 and FEU-60.

The high voltage was not the same for all the tubes. The R760 were sorted by gain and the FEU-60 and FEU-68 by noise level: for the ones with low noise the high voltage was chosen at the efficiency plateau. If the noise level was high and the tube had good gain, the high voltage was chosen so as to keep the noise low. The tubes were connected in sets of 16 to 20 cards[6]. These cards supplied high voltage for the tubes, low voltage for the amplifier/discriminator chips (+6.0 V and -5.2 V) and provided connectors

for readout cables which went to the latches. These cards were assembled in a *motherboard* as in Figure 3-b, which has card edge connectors to support the cards and distributes the low and high voltages required to each card. Four high voltage power lines were used: two -1250 V for the R760, -1700 V for the FEU-60 and -1800 V for the FEU-68, with 1 A fuses, and two low voltage power lines with 0.5 A fuses; all with their respective ground lines. For the R760 the current draw from the high voltage cable of each tube is approximately 200  $\mu$ A. For both the FEU-60 and FEU-68 tubes the current draw is in the range 120-170  $\mu$ A per tube.

Each card has a high voltage divider with a pad where 16 phototube high voltage cables were soldered. The output voltage was adjustable by 14 increments of 20 V (using Zener diodes) from one of the three negative input power supply voltages to 280 V below the input supply voltage. Both the output and the input high voltage selection were made by jumpers.

In Figure 4-a one card and the three different tubes are shown. Figure 4-b is a photograph of the photocathode.

The photocathode and readout were located in a small volume, a 30.5 cm radius by 36.8 cm deep cylinder (see Figure 1-a) which was, obviously, light tight. This volume was too small for adequate heat dissipation of the estimated load from the electronic components, about 200 W. A cooling

system[7] was installed to do this job. It consisted basically of fans and a chilled water heat exchanger. With this device the temperature inside the photocathode housing was around 26 C.

The digital signals were brought from the cards to the latch readout system through vacuum feedthroughs which used mass-terminated connectors mounted on circuit boards and then potted with epoxy. The hybrid chips have an analog output signal available from the preamplifier. For monitoring purposes one analog output was chosen from each card. These were routed to ADCs using standard BNC bulkhead feedthroughs.

### 1.3 Gas system

Before filling[8] the radiator vessel with neon and the photocathode volume with nitrogen, the counter was purged to reduce the gas contamination to an acceptable level ( $< 10^{-4}$  atm). The volumes were mechanically shorted together and pumped out simultaneously.

A different approach was used to fill it. As the two volumes in the RICH vessel were separated by a thin quartz window, a differential pressure gauge was installed to automatically keep the same approximate pressure on either side. The maximum difference,  $\Delta P$ , allowed was 1/4 inch of water. Gas flowed into one volume until the pressure difference between the two volumes

reached the maximum allowed value. Then the differential pressure gauge shut off gas flow to this volume and allowed gas to flow to the other one up to the same  $\Delta P$  level, and so on. The pressure in the radiator gas was set to be equal to the local atmospheric pressure and the volume was then sealed.

## 2 Detector response:

### 2.1 400 GeV/c $\pi^-$ beam

#### 2.1.1 Number of detected photons

By triggering on single tracks, events such as the one shown in Figure 5 were observed. A measure of signal to noise of the counter can be seen by examining the total number of hits in a region where photons were expected to be detected, the *expected ring region*, and the total number of hits outside of this region. Figures 6 show these two distributions, integrated over all tube types. From these data, it can be calculated that the probability of any individual tube to fire randomly in an event is  $4 \times 10^{-3}$ . In Figure 7 the performance of the three different tubes is shown, for tubes in and out of the *expected ring region*.

To track possible inefficiencies and/or noisy tubes an *off-spill monitoring system* was used. It consisted of either illuminating the tubes with an LED

(placed at the center of the photocathode array) or monitoring noisy tubes during pedestal events. A noisy tube was arbitrarily defined as one firing in more than 3% of the pedestal events. Typically this was fewer than 4 tubes in any run. These tubes were then flagged and eliminated in analysis of the beam-on data presented in Figure 7.

### 2.1.2 Figure of merit

A good way to characterize a Čerenkov Counter is by indicating its **Figure of Merit**,  $N_0$ . It is defined by the relation [9],

$$N_0 = \frac{N}{L \sin^2 \theta} \quad (1)$$

where  $N$  is the number of detected photons,  $L$  is the radiator length and  $\theta$  is the produced ring size. In order to measure  $N_0$  for each tube type, several corrections must be applied. These include accounting for the different angular coverage for each tube type, an adjustment for non-working tubes in the ring region and a subtraction for noisy tubes. Taking all these factors into consideration the E781 prototype detector behavior, as well as the tubes' Quantum Efficiency, is summarized in Table II.

Shown in Table III, taken from reference [10], which was updated to include more recent results, is a comparison of the E781 RICH prototype

performance to that of other working detectors.

## 2.2 Ring radius

As is well known[11], for a particle traversing the radiator medium with velocity  $\beta > 1/n$ , Čerenkov light is emitted at an angle  $\theta_C$  given by:

$$\theta_C = \arccos\left(\frac{1}{\beta n}\right); \quad \beta = \sqrt{1 - \frac{1}{\gamma^2}}, \quad (2)$$

where  $n$  is the refractive index (1.000067 for neon at 1 atm).

The ring radius at the focal plane of the mirror relates to the Čerenkov angle as

$$R = f \tan(\theta_C), \quad f \text{ is the focal length of the mirror.} \quad (3)$$

For a 10 m focal length this implies a very convenient relationship 1 cm = 1 mrad. In the small angle approximation

$$\theta^2 = 2\delta - \frac{1}{2\gamma^2} \quad (\delta = n - 1). \quad (4)$$

The fitted ring radius, shown in Figure 8, for a run with 10,000 events, was measured as

$$R = (11.314 \pm 0.0013) \text{ mrad}, \quad (5)$$

with a gaussian width

$$\sigma = (0.12829 \pm 0.00094) \text{ mrad}. \quad (6)$$

The stability of this detector was checked by measuring the ring radius as a function of time. Figure 9 shows the deviation from the nominal value for the ring radius for 13 runs taken over a 46 day period. One can see that it was stable at the 1% level.

The detector resolution calculated from the measured quantities (5) and (6) is given by

$$\frac{\sigma}{R} = 1.13\%. \quad (7)$$

This resolution should be sufficient to separate pions from kaons up to 250 GeV/c, as can be seen in Figure 10 in which the probability of identifying a K as a K, versus the probability of mis-identifying a  $\pi$  as a K, is plotted for different momenta for a detector with the observed resolution.

### 2.2.1 Detector resolution

In the focal plane of the RICH the rings are centered about the incident track direction, and the radius is given by equation (3).

Each phototube which fires gives an independent measurement of the ring radius

$$R_i = \sqrt{(\theta_i^x - \theta_t^x)^2 + (\theta_i^y - \theta_t^y)^2} \quad \sigma_i = \frac{s}{4} \quad (8)$$

where  $\theta_i^{x,y}$  are the angular coordinates of the  $i$ th PMT,  $\theta_t^{x,y}$  are the angles of the track,  $R_i$  is the ring radius determined by the  $i$ th PMT with resolution  $\sigma_i$ , and  $s$  is the angular size subtended by each PMT (1.5875 mrad). The resolution of each PMT is 0.40 mrad or 3.5% for a  $\beta = 1$  particle with the maximum ring radius of 11.34 mrad. For a ring with  $N$  PMTs the ring radius resolution is

$$R = \sum_{i=1}^N \frac{R_i}{N} \quad \sigma = \frac{s}{4\sqrt{N}} \quad (9)$$

For the average of 11.77 PMTs per event observed in this prototype the ring radius resolution is 0.116 mrad or 1.02% for a  $\beta = 1$  particle. This dominant contribution to the resolution is determined strictly by the geometry of the phototube array.

The track angular resolution is better than 0.10 mrad and the mirror focal length is known to about 1%, justifying their contribution to the resolution being negligible. Other contributions to the ring radius resolution come from the physics of producing and transporting the Čerenkov photons

to the PMTs. Multiple Coulomb scattering of the particles in the spectrometer and RICH is  $<0.05$  mrad for particles above 50 GeV/c. The dispersion in neon is 0.105 mrad averaged over the detected Čerenkov spectrum. Optical aberrations are negligible for the optical quality mirror used in this test. Finally, the RICH angular coordinate system must be aligned with the coordinate system of the magnetic spectrometer system. The uncertainties in this alignment are a systematic error. A summary of all the contributions to the resolution for  $\beta = 1$  particles is given in Table IV.

The contribution of tube noise is estimated from the observed noise probability per tube of 0.0043. The relative efficiency of the light cones was estimated to be 80%. This improves the geometrical resolution  $\sigma/4 = 0.397$  to the 0.375 value used in Table IV since photons with the worst resolution are lost. The calculated resolution is slightly worse than that observed from the fit to the ring radius distribution shown in Figure 8. This small difference is likely due to the light cone efficiency being somewhat overestimated. If that efficiency were 67% the predicted resolution would agree with the observed value.

## 2.3 Momentum Scan

The  $\pi$ , K and p separation was studied by taking data at different beam momenta.

Figure 11 shows the detector performance for -175 GeV/c beam, with a two gaussian fit to the ring radius data. The arrows indicate cuts which would give either 99% or 90% pion rejection (and correspondingly, 49% or 89% kaon acceptance). This is in good agreement to the prediction of Figure 10, as are similar data at other momenta.

Summarizing the measurements of the momentum scan, the ring radius behavior as a function of the beam momentum calculated from the 3 PWC stations is shown in Figure 12.

The resolution as a function of momentum and particle type is shown in Figure 13-a and as a function of measured ring radius in Figure 13-b. The worsened resolution at smaller ring radii is due to the fact that the number of photons produced, and thus detected, goes with  $\theta^2$ .

The relative fraction of  $\pi$ , K and p, defined as the number of particles of each kind compared to the total number of detected  $\pi$ , K and p has also been determined. For a negative beam, the result is given in Figure 14.

## 2.4 Multiple tracks

Near the end of the run a target was placed in the 400 GeV/c  $\pi^-$  beam in order to produce multi-track events. It is clear that for a RICH detector to work, it has to be able to sort out rings from multiple tracks which may be overlapping.

For this data, the particle trajectories (determined from the PWCs and Silicon Microstrip Detectors in this configuration) were projected onto the photocathode to give the centers of the rings. Then the  $\pi/K/p$  hypotheses were tested by fitting the appropriate rings for the particles' measured momenta.

Shown in Figures 15-a, b and c are three examples of two and three particle reconstructed trajectories and the produced rings in the prototype RICH.

Figure 15-d is a selected event with all three hypotheses shown for track number 1, with momentum 226.5 GeV/c, and only the pion hypothesis for track 2, with momentum -141.6 GeV/c. For track 1, the fitted radius, 10.63 mrad, is within one sigma of the prediction for a proton (10.72 mrad), and greater than five sigma away from the kaon or pion prediction. For track 2, the fitted radius, 11.38 mrad, is well within one sigma of the prediction for a pion (10.45 mrad), and 3.36 (7.73) sigma away from the kaon (proton)

prediction.

### 3 Conclusions

A prototype RICH detector with a phototube-based photocathode array has been successfully tested, utilizing three different phototubes in the array. For 400 GeV/c  $\pi^-$ , 11.8 photons per ring were detected and the ring radius resolution obtained was 1.13%. This is sufficient to provide useful separation of pions and kaons up to 250 GeV/c.

### 4 Acknowledgements

The collaboration wants to thank the E800 experiment for granting us beam time, Fermilab Site Operations Vacuum Group, Fermilab Mechanical Department and Fermilab Physics Department for their contributions to this prototype, and the administrations of the Institute of High Energy Physics, Serpukhov and Moscow State University for their support of this project and the group from Petersburg Nuclear Physics Institute for the readout system. Special thanks to the other members of the E781 collaboration who helped during the test run data taking.

	Tube diameter	Photocat diameter	Window material	Dynodes	Q.E. <sup>a</sup> (%)	Maximum voltage
<b>R760</b>	13.5 mm	10 mm	Quartz	10	25	-1250 V
<b>FEU-60</b>	15 mm	10 mm	Glass	10	10	-1700 V
<b>FEU-68</b>	15 mm	10 mm	Glass	10	9	-1800 V

<sup>a</sup>Quantum Efficiency

**Table I - Characteristics of each tube type.**

	Q.E.(%)	$N_0(cm^{-1})$
<b>R760</b>	23.4	$154.6 \pm 5.4$
<b>FEU-60</b>	11.2	$72.3 \pm 3.3$
<b>FEU-68</b>	9.9	$66.1 \pm 2.7$

**Table II** - Measured Quantum Efficiency and Figure of Merit for the three different tubes.

Table III - RICH counters working for physics

Experiment	In use	Beam	Physics	Radiator	Mirror /	Window	Photoion.	Detector gas	Headout				
									X, Y, Z	Electr.	$N_{ph}$	$N_0(\text{cm}^{-1})$	
<i>Fixed target</i>													
E605/789 RICH	82-84/90	p	dihadrons/ B $\rightarrow$ h $\bar{h}$ , f $\bar{f}$	He/A	8 m (16 m rad.)	CaF <sub>2</sub>	TEA	He/CH <sub>4</sub>	wire, wire, -	ADC	5	43	
$\Omega$ RICH	84-86/90	$\gamma/\Sigma\Xi\Omega$	photoprod/ hyperons(c)	N <sub>2</sub> /C <sub>2</sub> F <sub>6</sub>	5 m	SiO <sub>2</sub>	TMAE	CH <sub>4</sub> /C <sub>2</sub> H <sub>6</sub>	wire, drift, -	TDC	12	40	
E665 RICH	88, 90	$\mu$	deep incl.	A/He	5 m	CaF <sub>2</sub>	TEA	CH <sub>4</sub>	pad, pad, -	FADC	5	17	
NA45 RICH	90	<sup>32</sup> S	e <sup>+</sup> e <sup>-</sup> prod.	CF <sub>4</sub> CH <sub>4</sub>	1.3 m 4 m	CaF <sub>2</sub> SiO <sub>2</sub>	TMAE	He/C <sub>2</sub> H <sub>6</sub>	pad, pad, -	ADC	10 11	112 65	
<i>Colliders</i>													
UA2 RICH	85-86	p $\bar{p}$	$\sigma_c^{tot}$	C <sub>2</sub> F <sub>6</sub>	0.6 m	CaF <sub>2</sub>	TMAE	C <sub>2</sub> H <sub>6</sub>	wire, drift, pad	TDC	4	40	
DELPHI RICH	90	e <sup>+</sup> e <sup>-</sup>	SM, asym., B	C <sub>2</sub> F <sub>12</sub> C <sub>6</sub> F <sub>14</sub>	0.6/0.4 m	SiO <sub>2</sub>	TMAE	CH <sub>4</sub> /C <sub>2</sub> H <sub>6</sub>	wire, drift, pad	TDC	14 <sup>a)</sup>	36	
SLD CRID	91	e <sup>+</sup> e <sup>-</sup>	SM, asym.	C <sub>2</sub> F <sub>12</sub> C <sub>6</sub> F <sub>14</sub>	0.6/0.4 m	SiO <sub>2</sub>	TMAE	CH <sub>4</sub> /C <sub>2</sub> H <sub>6</sub>	wire, drift, ch. div.	FADC	-	-	

a) For specification, see the paper contributed by E.G. Anagnostis et al. (DELPHI Barrel Group) to the IEEE Nuclear Science Symposium, 1990

Update to Above Table

Experiment	In use	Beam	Physics	Radiator	Mirror /	Window	X,Y,Z	Electr	Nhit	$N_0(\text{cm}^{-1})$
SPHINX	89-91	$\pi$ , K, p	Exotic hadronic states	SF <sub>6</sub>	1.25 m	-	PMTs	Latch	13.7	60

E781T	91-92	$\pi^-$	Test run	Ne	10 m	SiO <sub>2</sub>	PMTs	Latch	11.8	93
-------	-------	---------	----------	----	------	------------------	------	-------	------	----

E781	To be built	$\pi$ , K, p	Charmed baryon studies	Ne	10 m	SiO <sub>2</sub>	R760	Latch	20	154
							FEU-60	Latch	9	72
							FEU-68	Latch	8	66

Source	Resolution (mrad)	$\sigma/R$ (%)
Phototube Array Geometry/PMT	0.375	3.32
Dispersion in Ne/PMT	0.105	0.93
TOTAL per PMT	0.390	3.44
TOTAL per ring (11.77 PMTs)	0.114	1.00
Spectrometer resolution	0.056	0.49
Particle multiple scattering	0.010	0.09
PMT noise	0.039	0.34
Total	0.133	1.17
Observed	0.128(1)	1.13

**Table IV** - Contributions to the detector resolution for 400 GeV/c particles.

## References

- [1] J. Séguinot and T. Ypsilantis, Nucl. Instrum. Methods **142** (1977) 377.
- [2] The spread in the observed Čerenkov angle due to the dependence of the refractive index of the gas on the produced photons' energy. See, for example, for more details, T. Ekelöf, Proceedings of the 12th SLAC Summer Institute on Particle Physics, **244** (1984); J. Séguinot, CERN-EP/89-92, LPC/89-25, Course given at *l'École Joliot-Curie*.
- [3] This vessel was used in experiment E756 and adapted for the E781 test run.
- [4] Eight R760 tubes were pressurized to 3 atm of neon for one month. The residual gas in the tubes was then checked, showing a degradation in the vacuum. Hamamatsu Photonics K.K., private communication.
- [5] I. Filiminov, L. Landsberg, V. Molchanov, A. Nemitkin, V. Rud, V. Solyanik, Internal note, 1991.
- [6] The cards were built by the Fermilab Physics Department.
- [7] The cooling system was designed and built by the Fermilab Mechanical Department.

- [8] This new gas filling system is a design and implementation of the Fermilab Site Operations Vacuum Group.
- [9] See, for example, references [1], [2], and J. Litt and R. Meunier, *Annu. Rev. Sci.* **23** (1973) 1.
- [10] T. Ekelöf, *IEEE Transactions on Nuclear Science*, Vol. **38**, No **2**, (1991) 424.
- [11] J. Litt and R. Meunier, in reference [9].

## Figure Captions

1. a) RICH prototype layout; b) Experimental E781 test run setup.  
(Not to scale.)
2. The tube holders with light-gathering cone. (Units are inches.)
3. a) The photocathode array showing how the three different kinds of tubes were arranged. The ADC symbol indicates a tube for which an additional analog signal was read out for monitoring. An LED was located in the center of the matrix, also for monitoring purposes. The blank holes were uninstrumented. b) The *motherboard* and the *cards*. (Not to scale.)
4. a) One card and the three different tubes is shown. b) The photocathode fully assembled. The R760 and FEU-60 are shown here. The hybrid chips can be seen on the cards.
5. A single event display in which 13 photons were detected. The cross is the center of the fitted ring and the diamond represents the projected particle trajectory.
6. a) The distribution of the total number of tubes which fired per event in the expected ring region. b) The distribution of the number of noisy tubes per event.

7. For each tube type: The distribution of the total number of tubes which fired per event in the expected ring region: a) R760, c) FEU-60, e) FEU-68; and the distribution of the number of noisy tubes per event: b) R760, d) FEU-60, f) FEU-68.
8. The average fitted ring radius for a -400 GeV/c beam.
9. The deviation from the expected ring radius measured over a 46 day period.
10. The probability of identifying a K as a K versus the probability of mis-identifying a  $\pi$  as a K, for various momenta.
11. Fitted ring radius distribution measured for -175GeV/c. Also shown is a two gaussian fit to the data. The fraction of pions rejected by various cuts is indicated by the arrows.
12. Measured ring radius as function of momentum for  $\pi^-$ ,  $K^-$  and  $\bar{p}$ .
13. Measured ring radius resolution as a function of a) momentum for  $\pi^-$ ,  $K^-$  and  $\bar{p}$  and b) ring radius.
14. Relative measured fraction of  $\pi^-$ ,  $K^-$  and  $\bar{p}$  as a function of momentum.
15. a), b), and c) show two and three-track events. In Figure d) a two track event is shown. For track 1 the three hypotheses,  $\pi$ , K and

p are shown, with a clear match to the proton hypothesis. For track 2, only the  $\pi$  ring is shown.

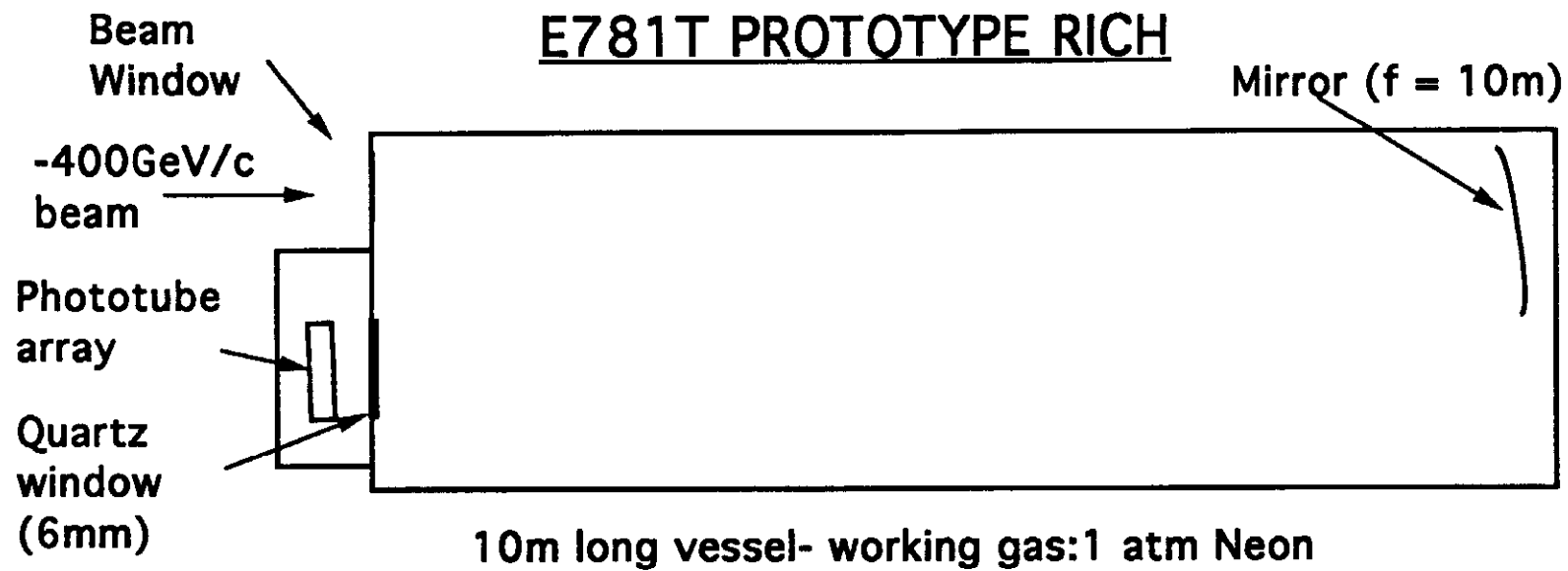


Figure 1 - a

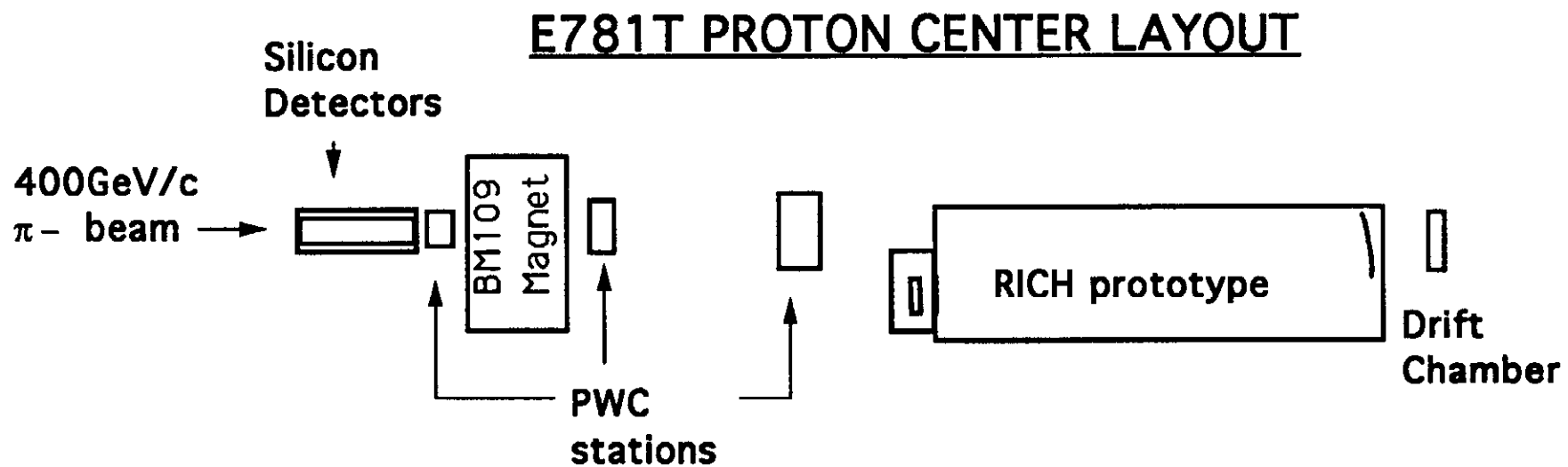


Figure 1 - b

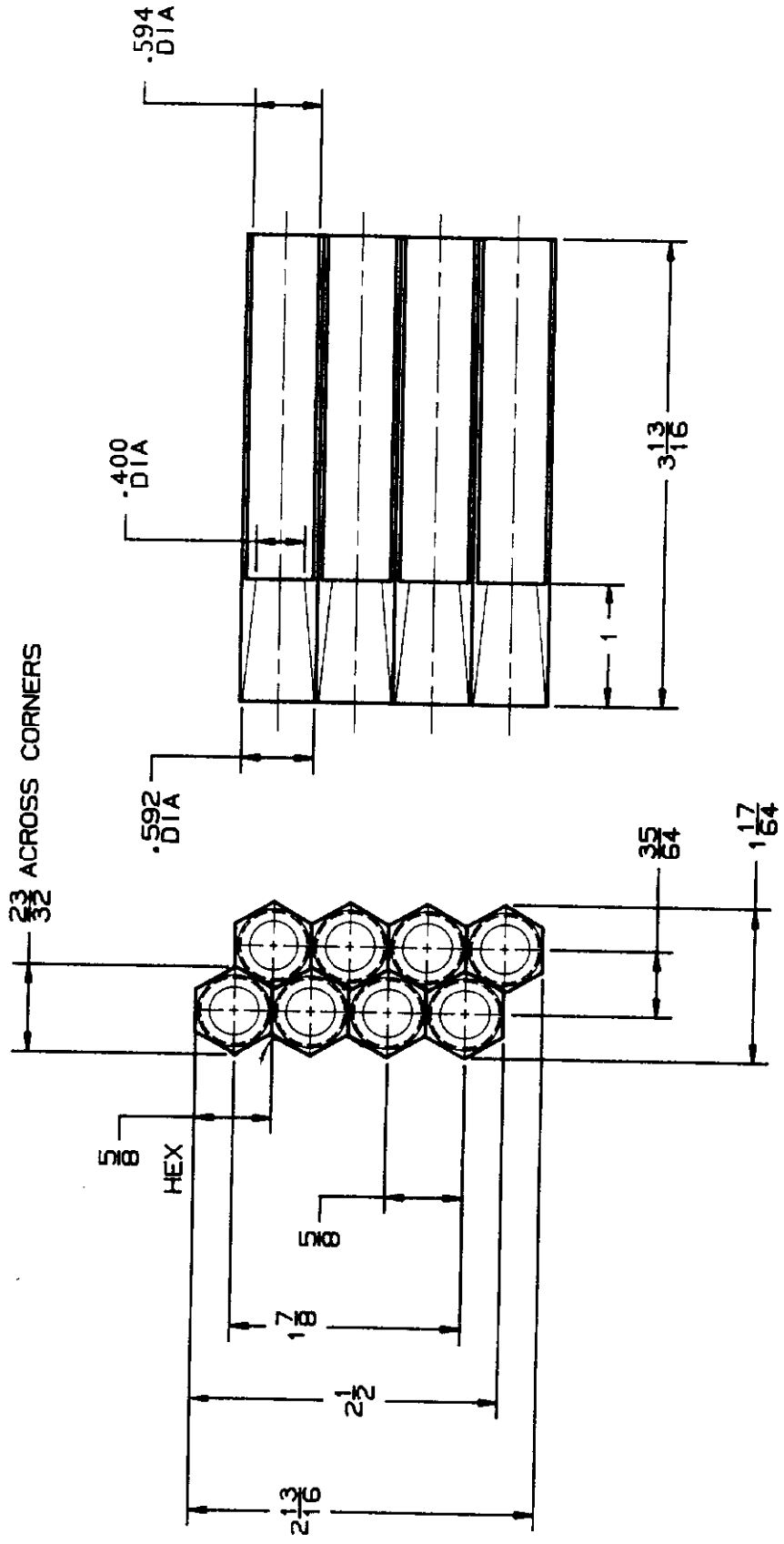


Figure 2

# RICH Photocathode Layout

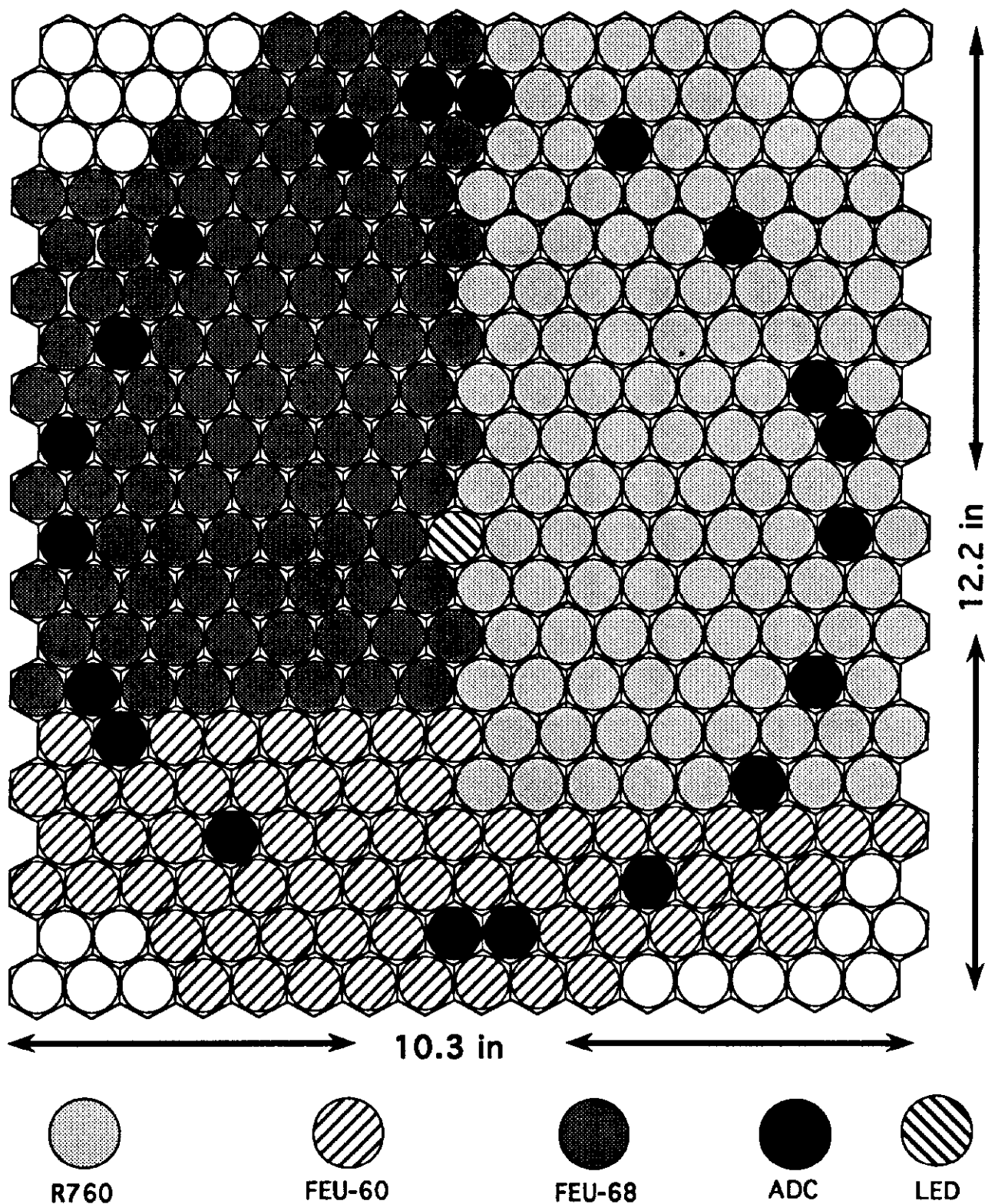


Figure 3 - a

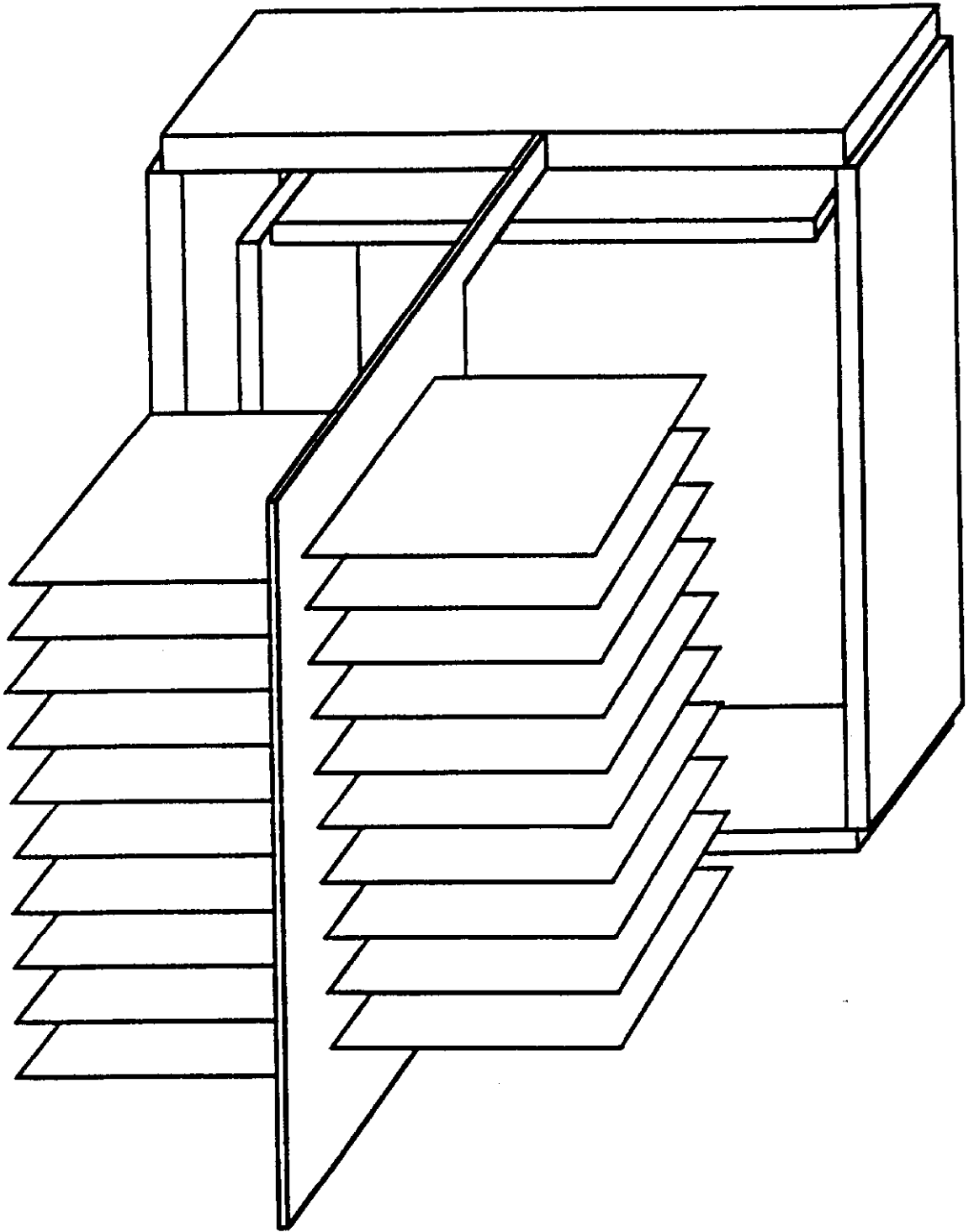
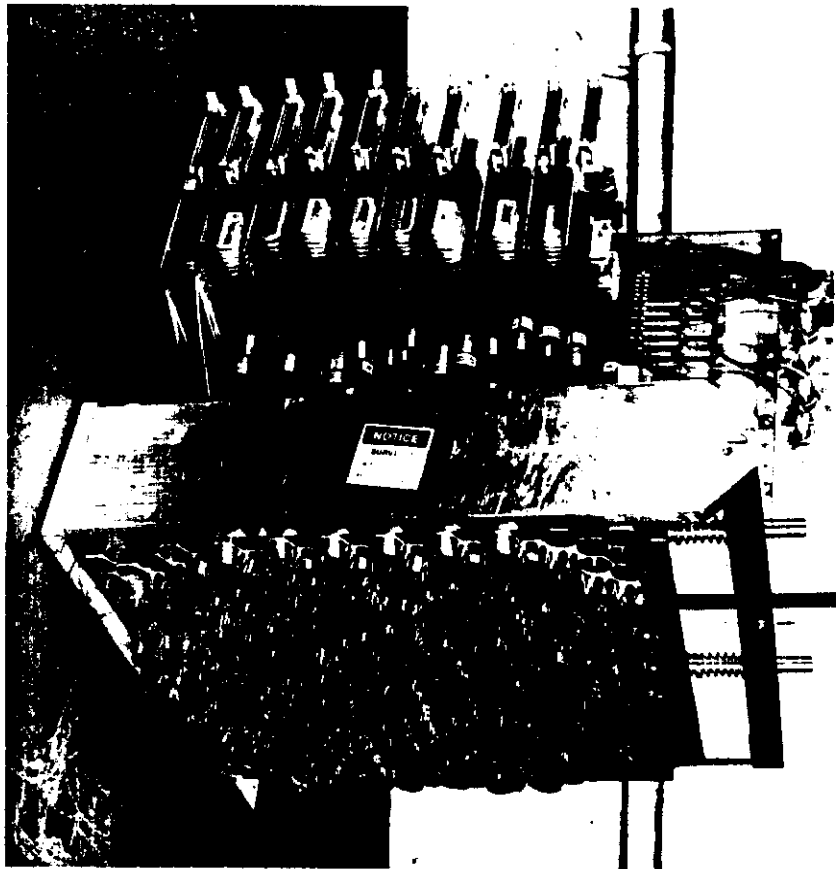
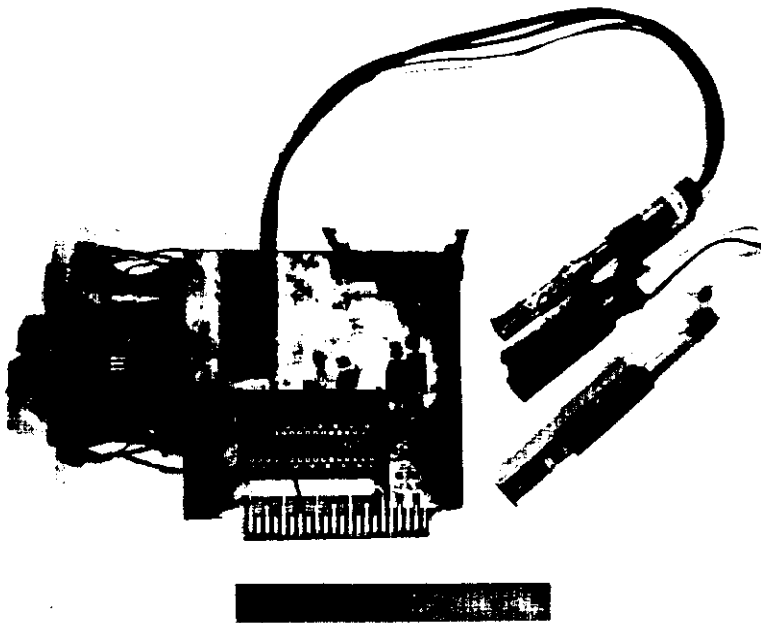


Figure 3 - b



4-  
201

Run 1593 Event 30690

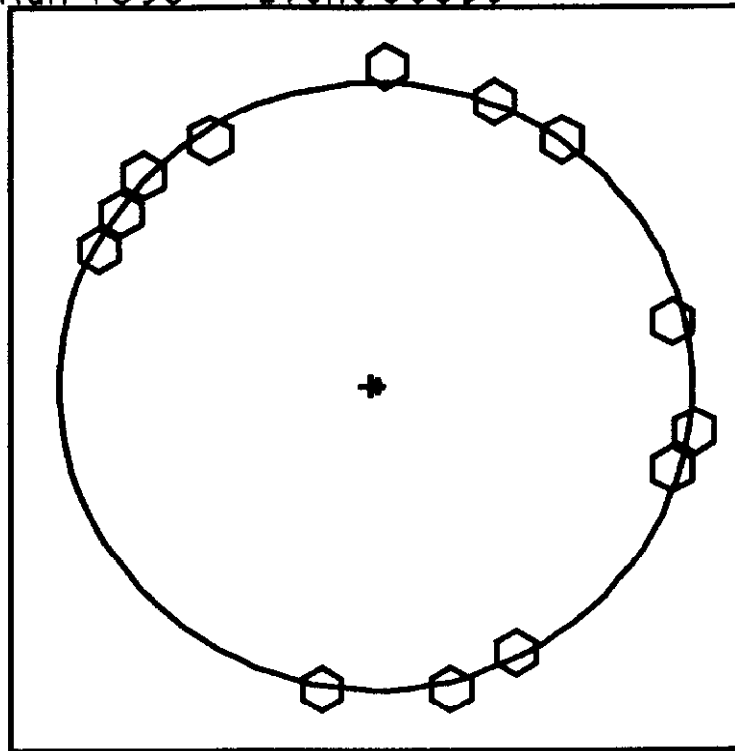


Figure 5

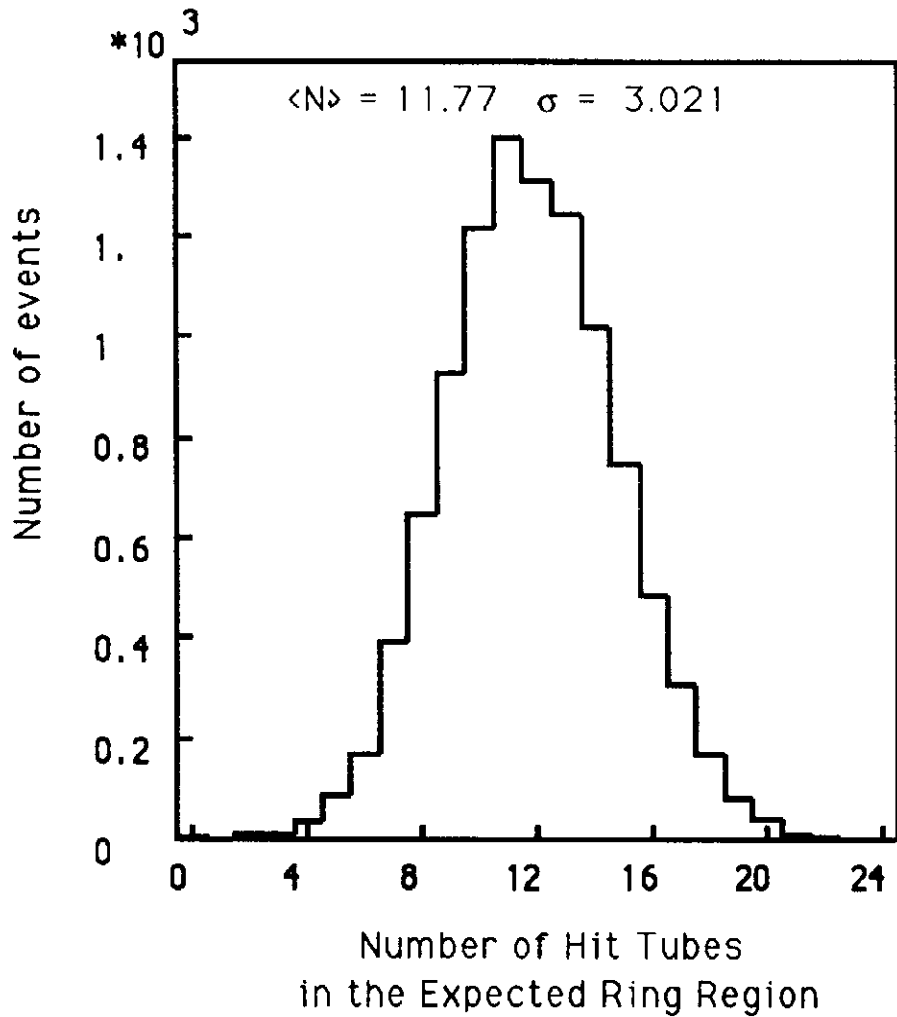


Figure 6 - a

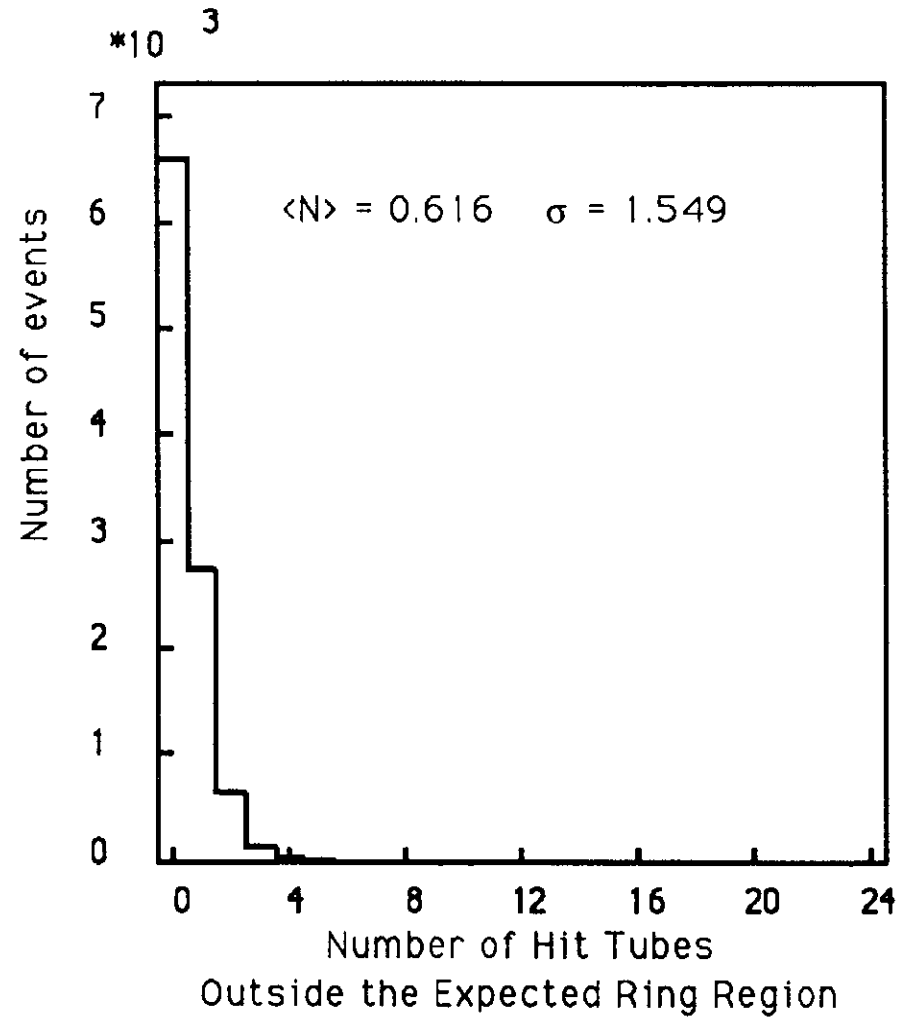


Figure 6 - b

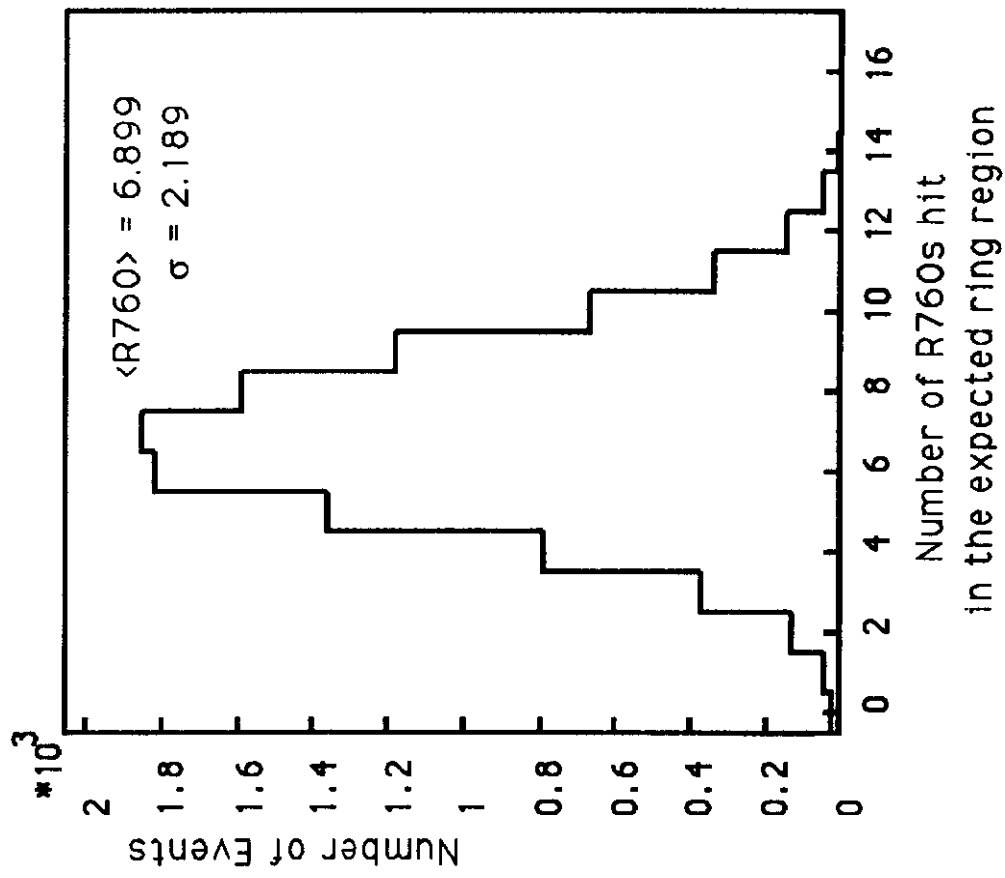


Figure 7 - a

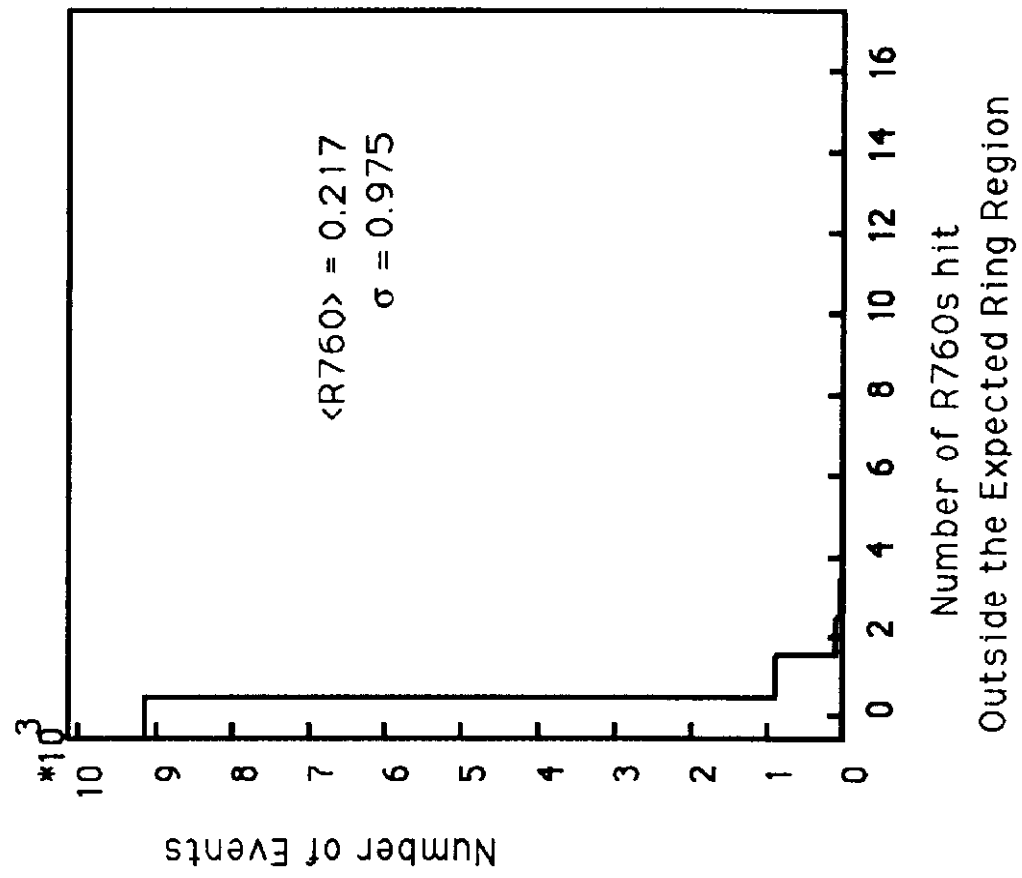


Figure 7 - b

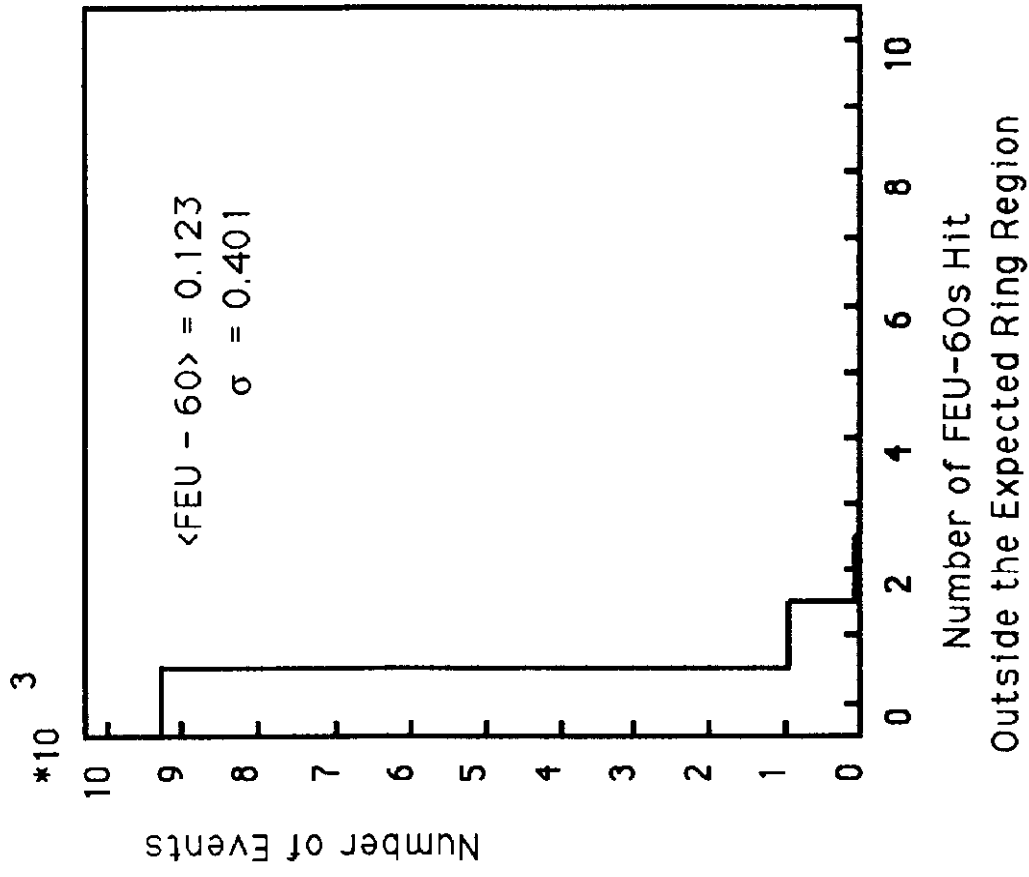


Figure 7 - d

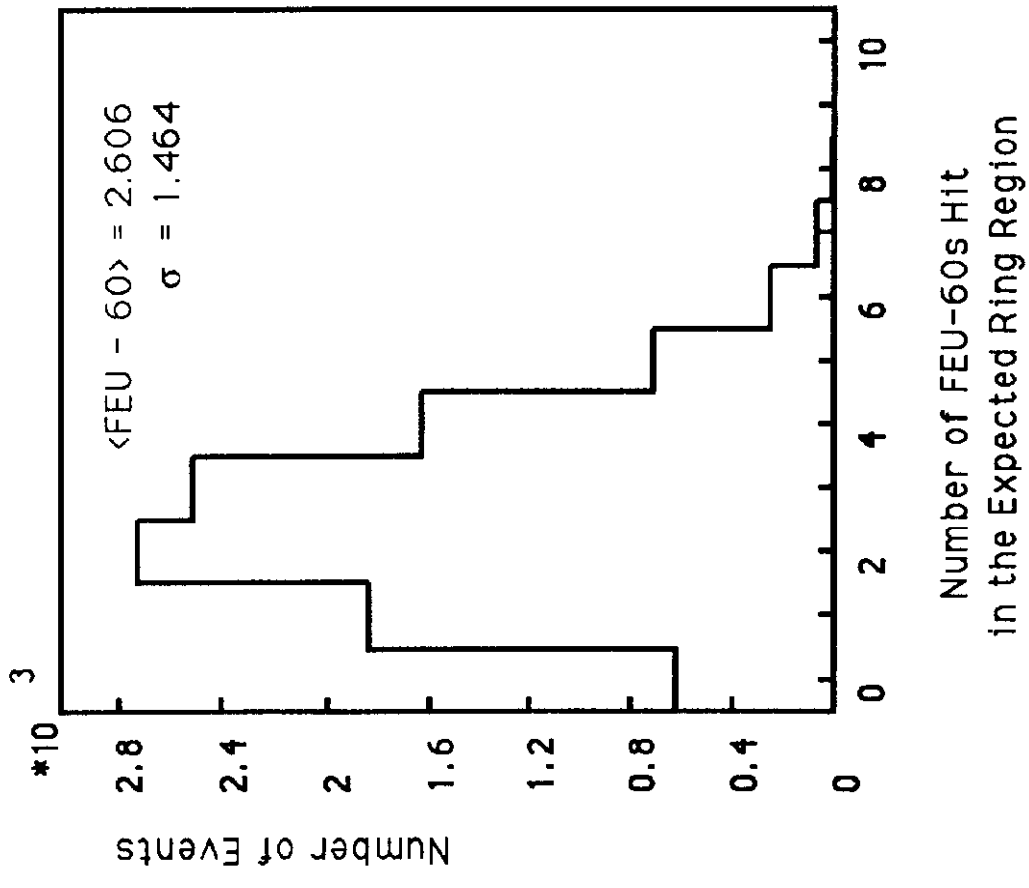


Figure 7 - c

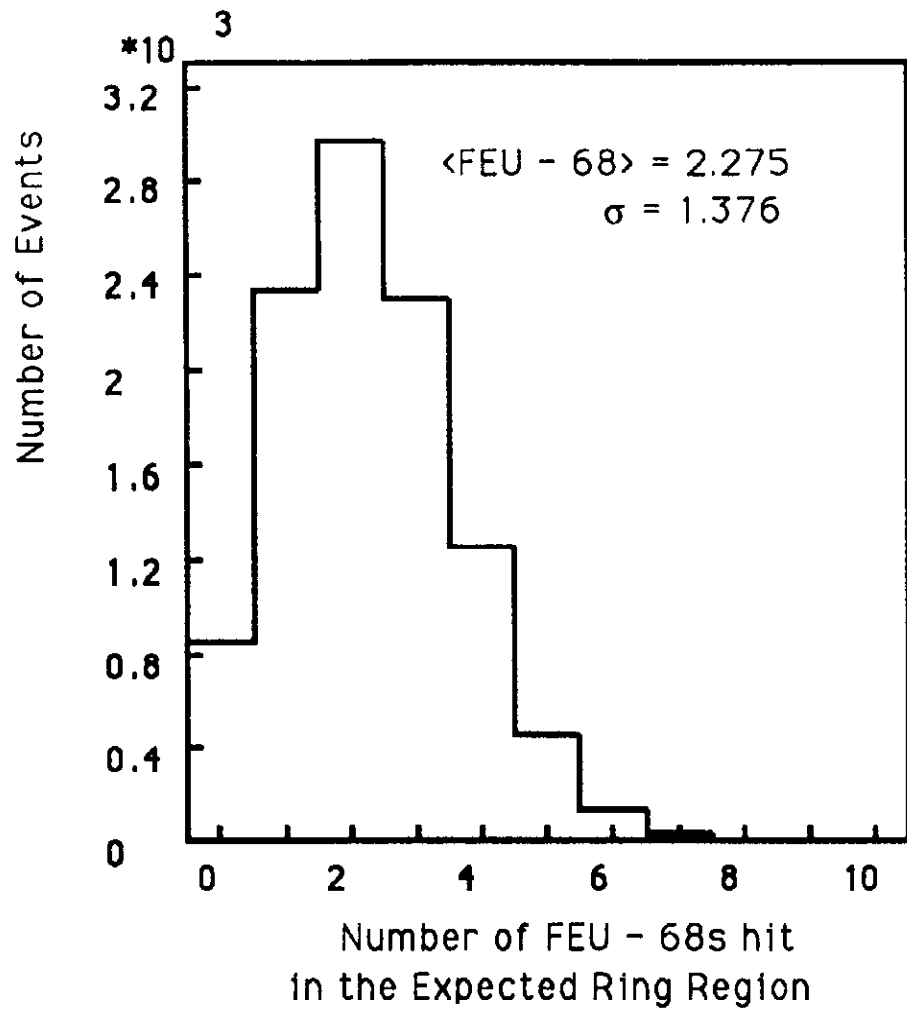


Figure 7 - e

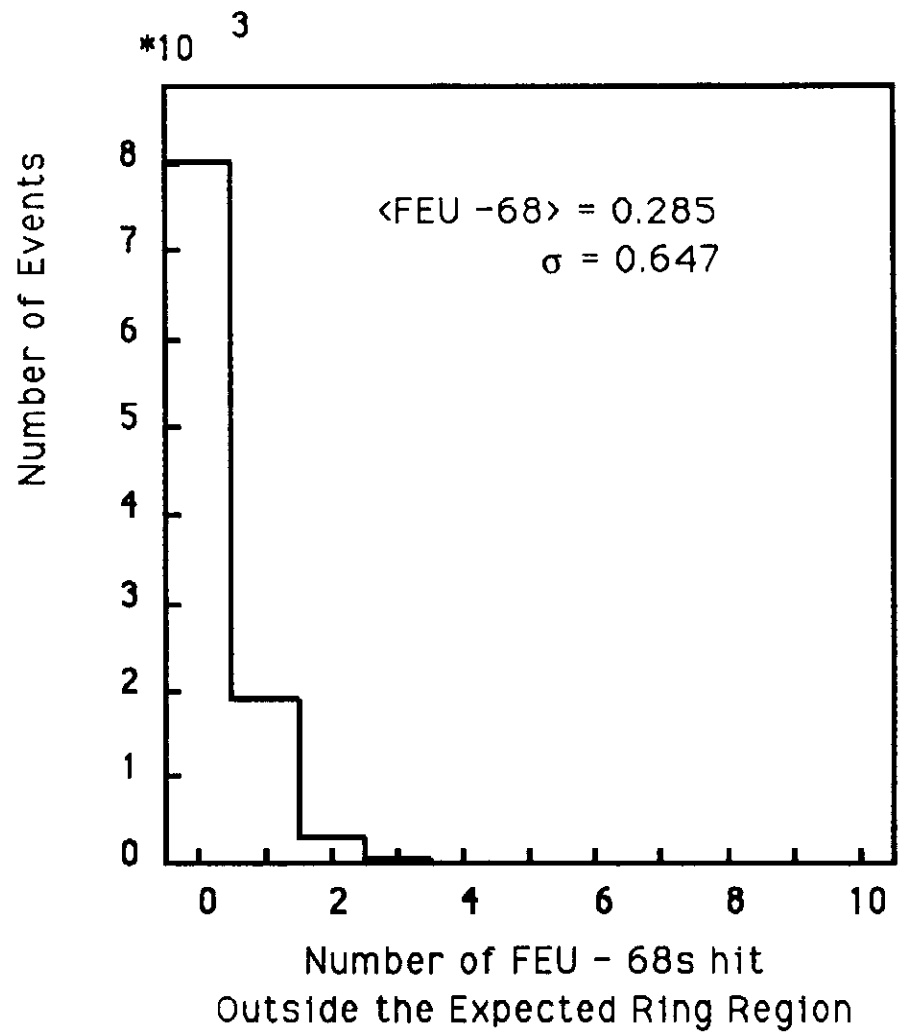


Figure 7 - f

### Fitted Ring Radius for -400 GeV/c Beam

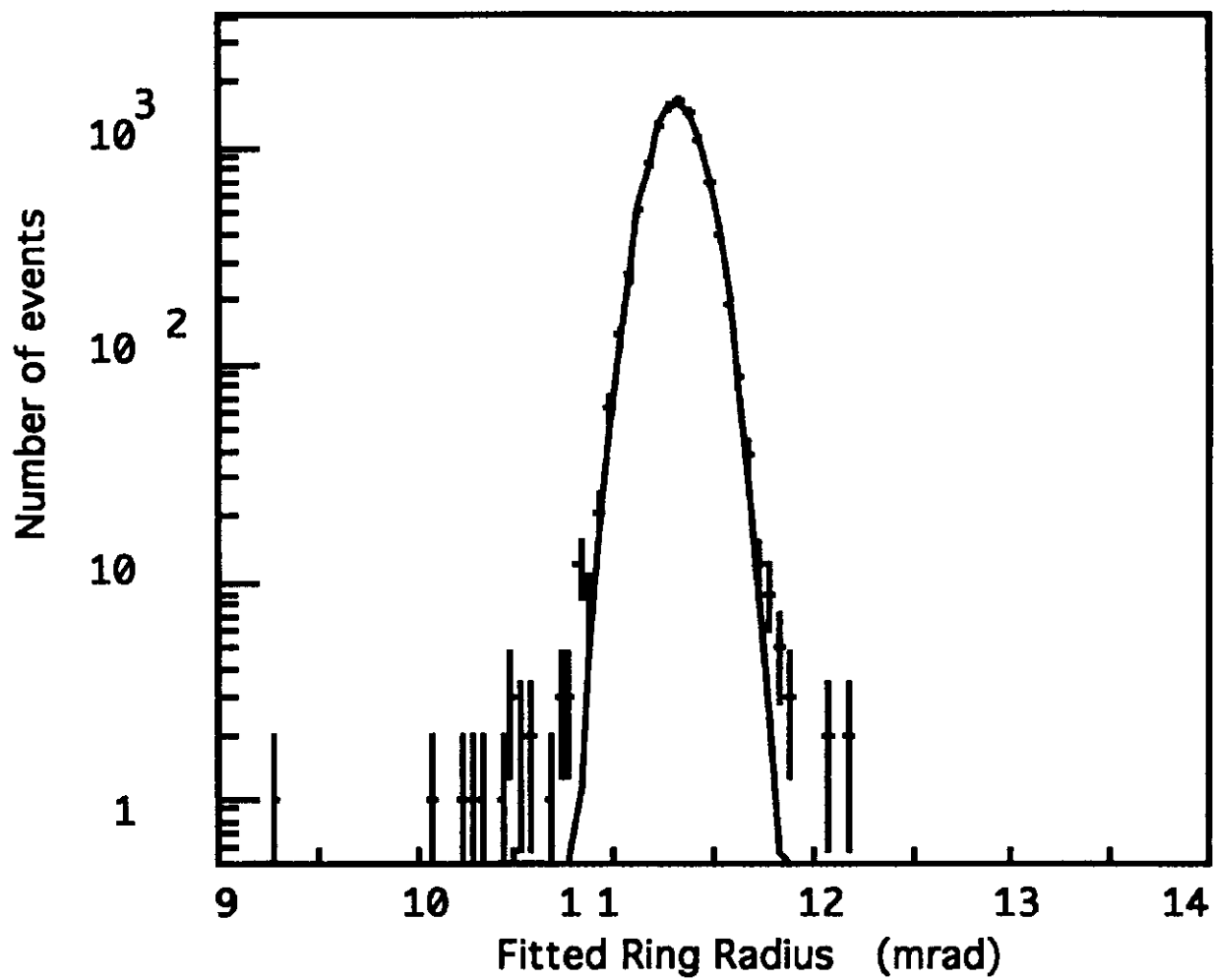
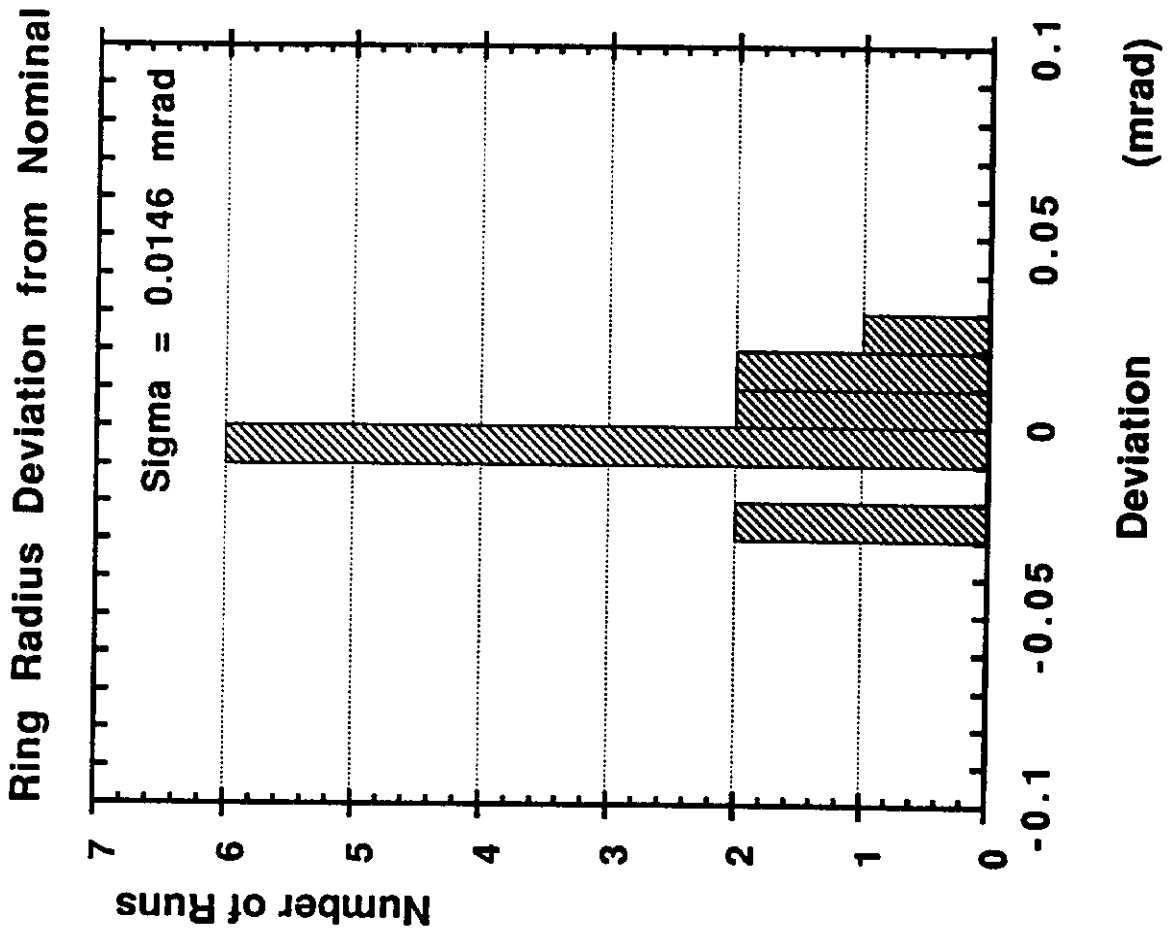


Figure 8



**Figure 9**

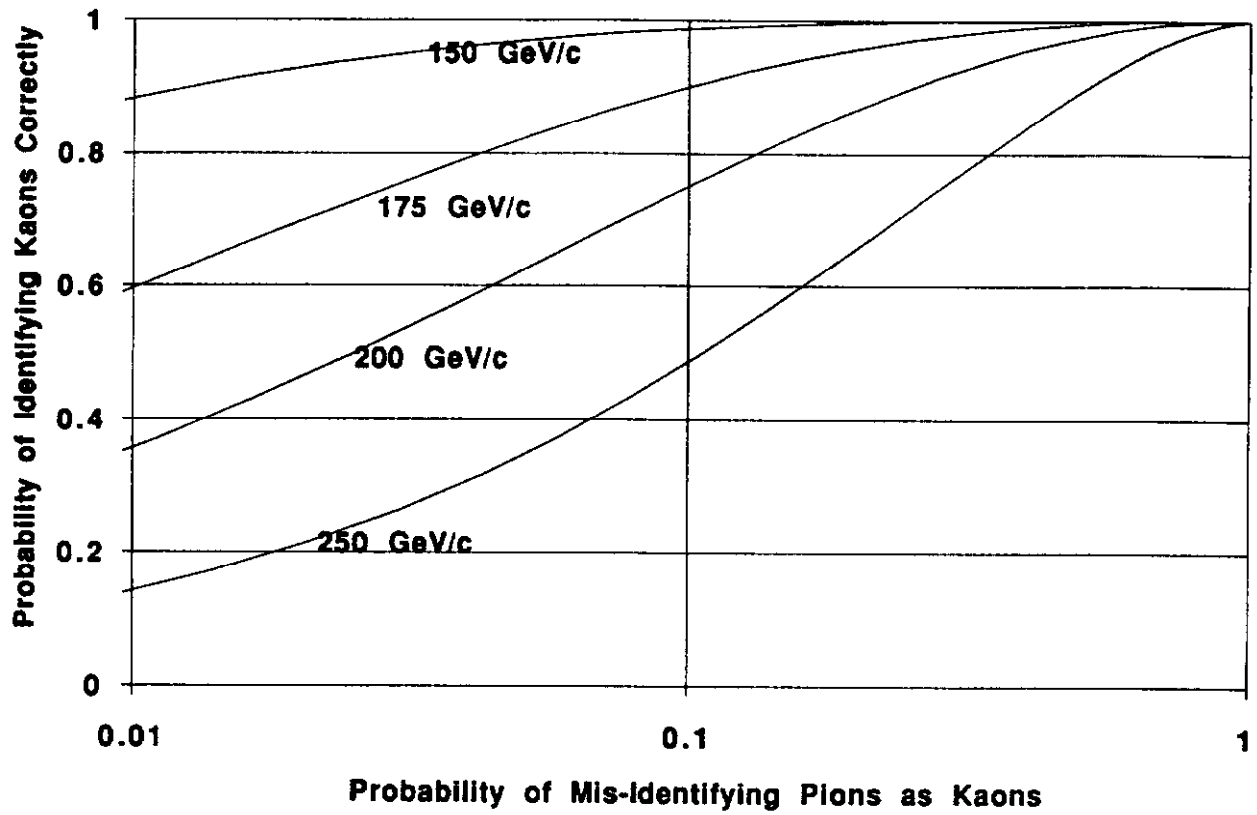


Figure 10

# -175 GeV/c $\pi$ /K Separation

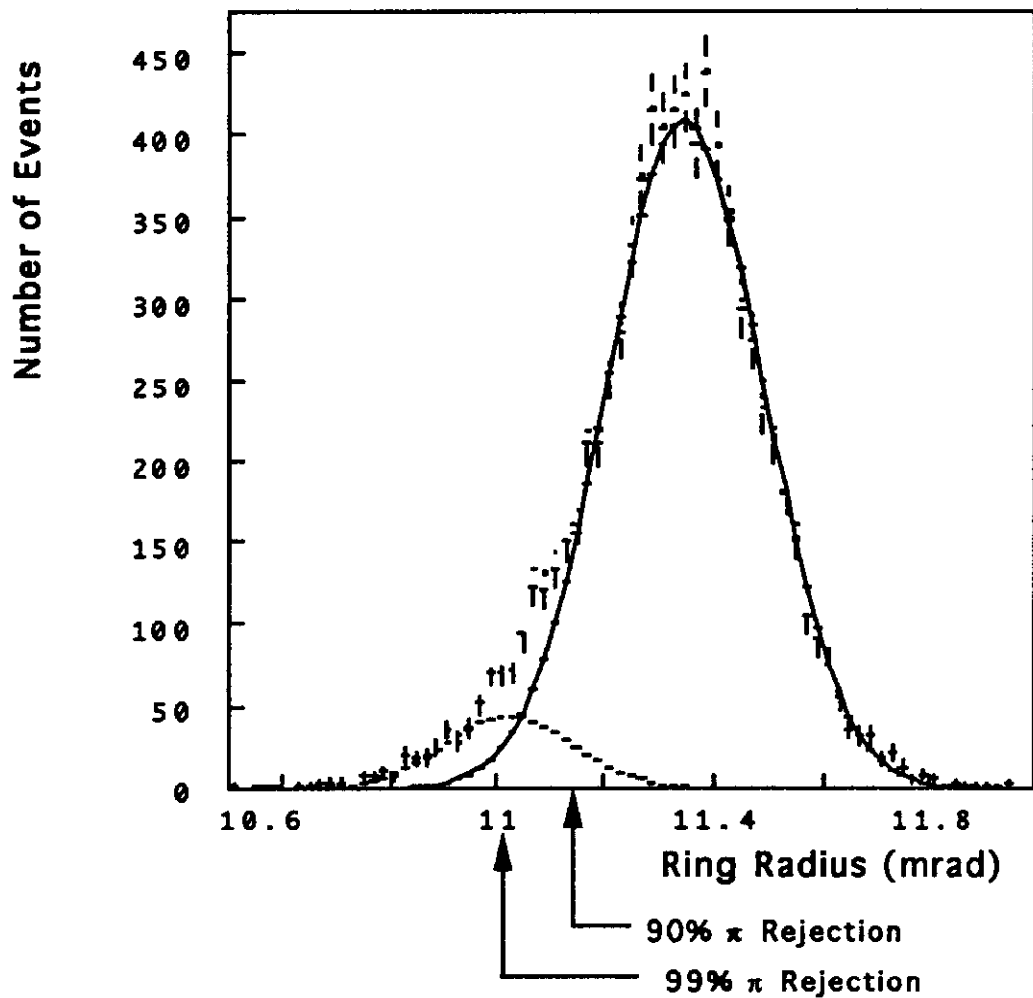
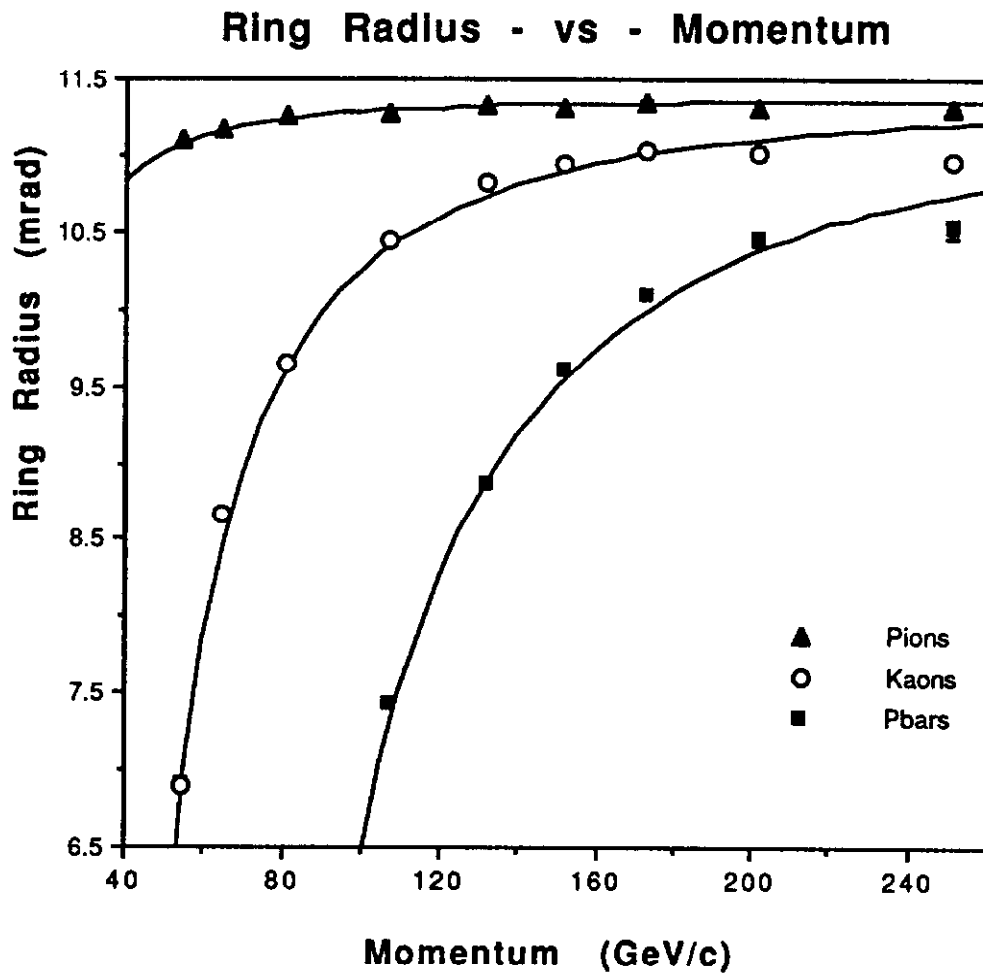
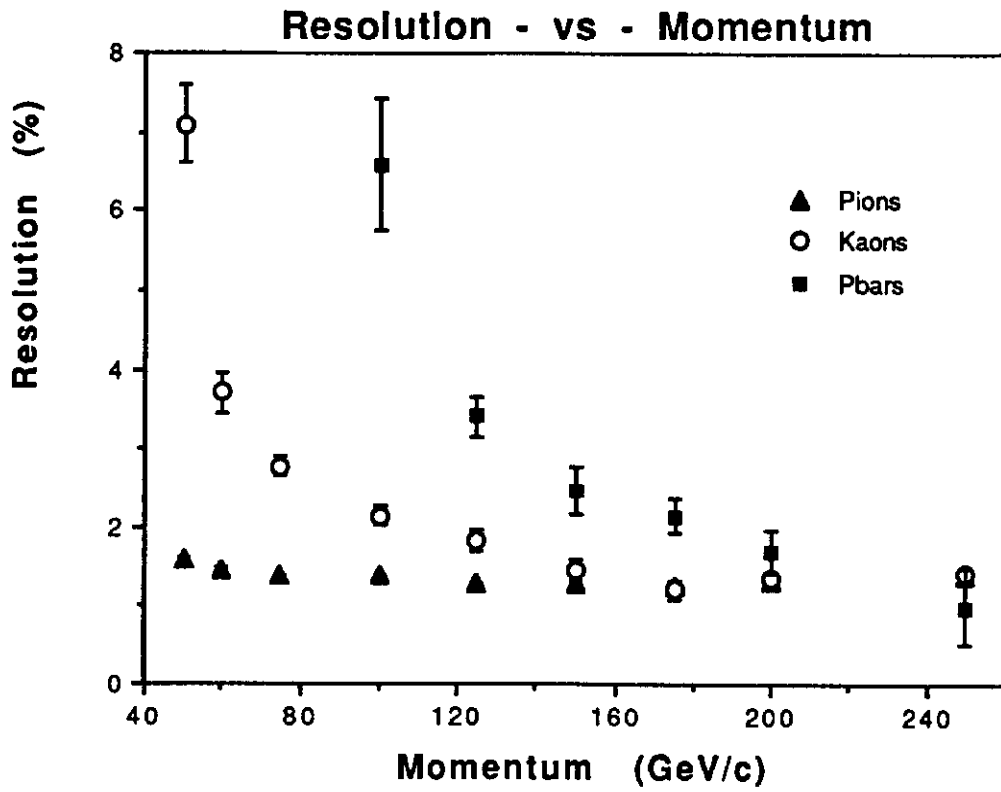


Figure 11



**Figure 12**



**Figure 13 - a**

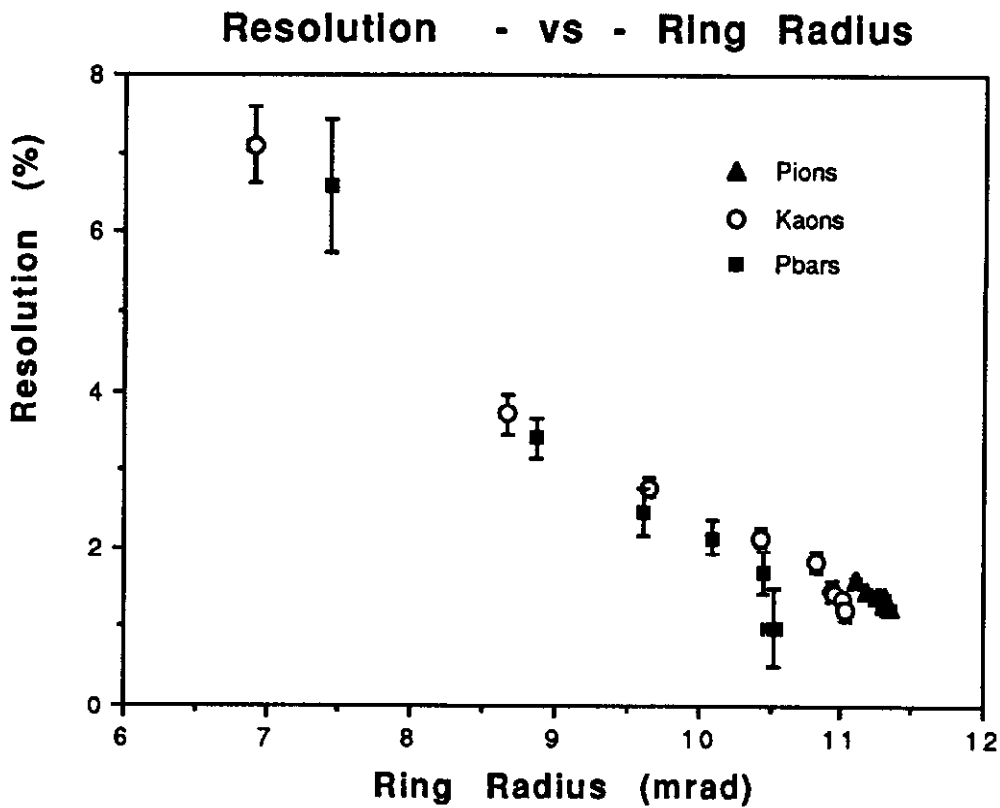


**Figure 13 - b**

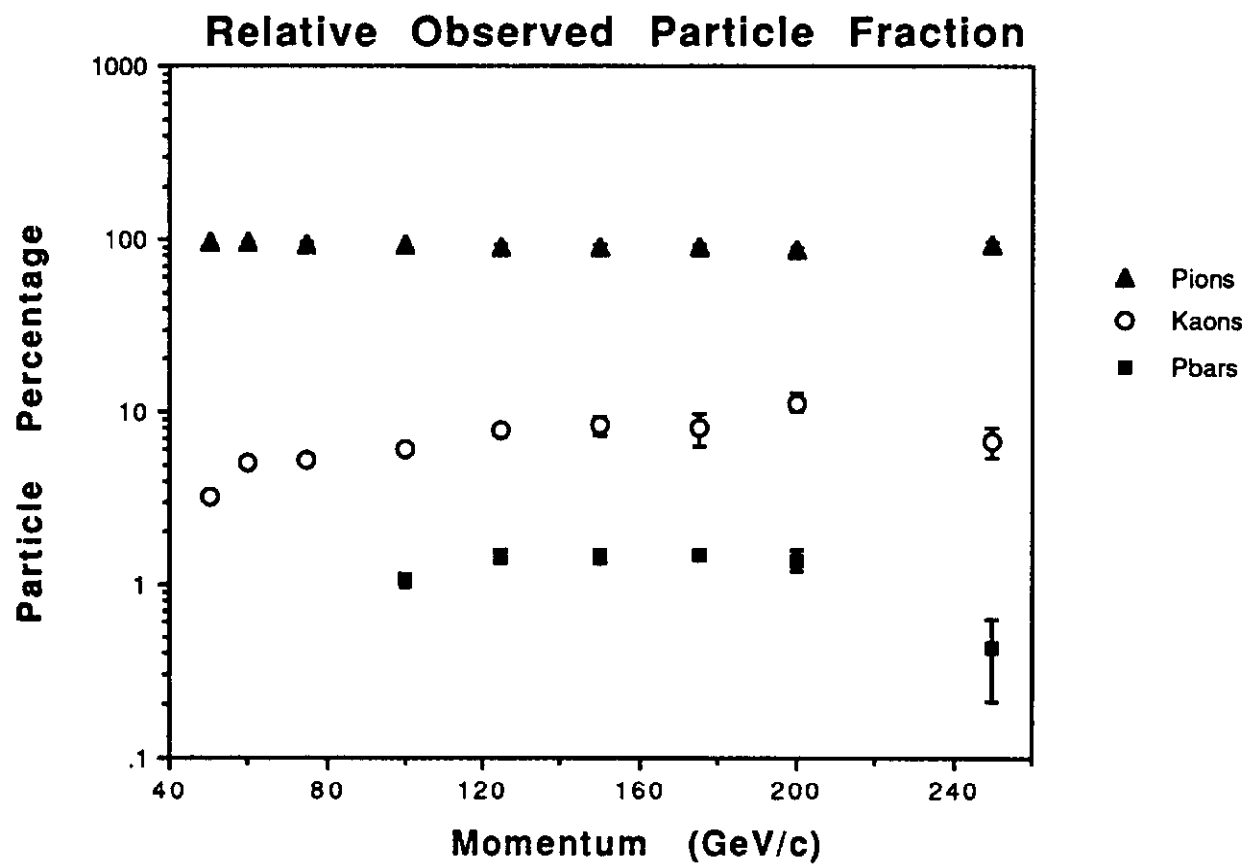


**Figure 14**

Event 29587

+: 173.7 GeV/c  
X: -141.9 GeV/c

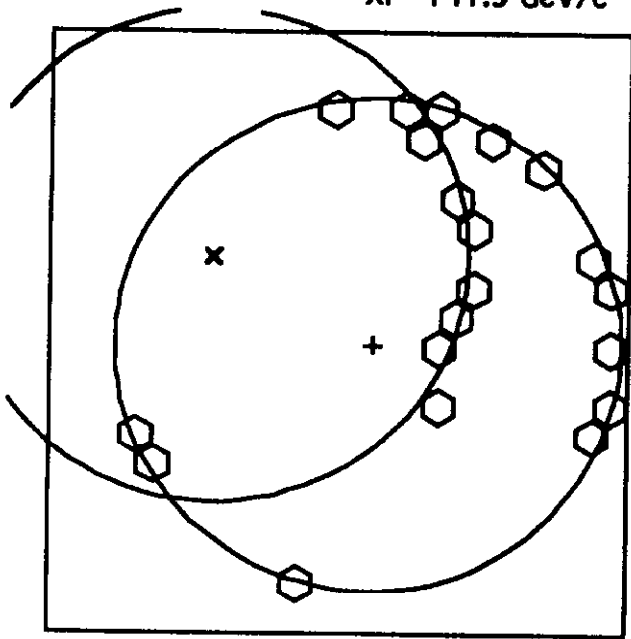


Figure 15 - a

Event 15671

+: 389 GeV/c  
X: -81.7 GeV/c

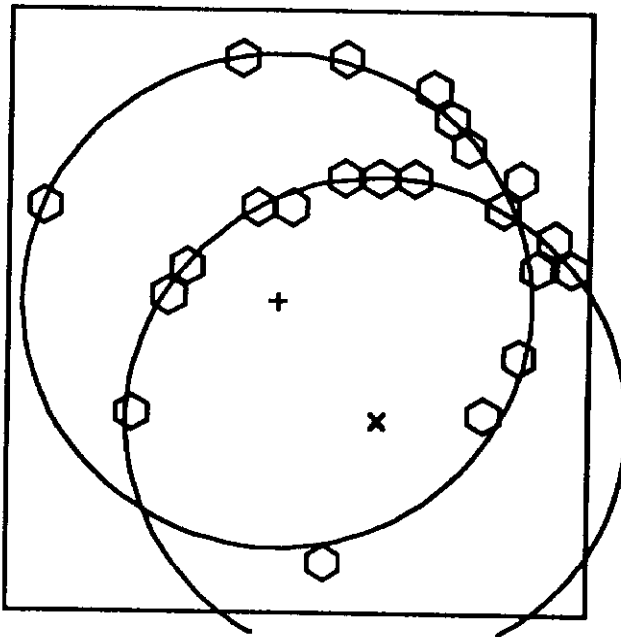


Figure 15 - b

Event 16957

+: -216.4 GeV/c  
X: - 64.8 GeV/c  
⊗: 53.8 GeV/c

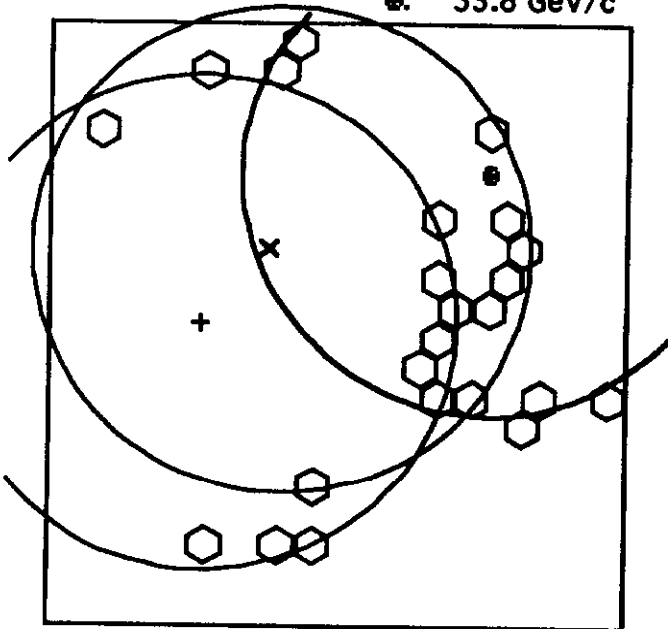


Figure 15 - c

Event 26063

1: + 226.5 GeV/c  
2: X -141.6 GeV/c

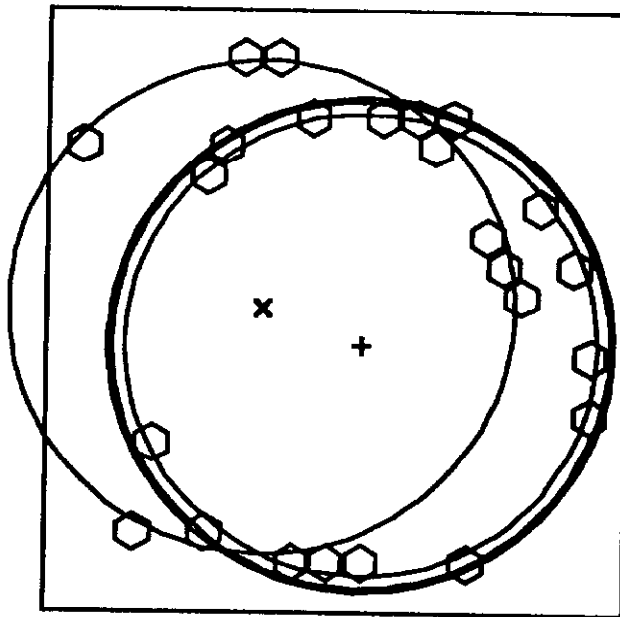


Figure 15 - d